HHS Public Access

Author manuscript

J Invest Dermatol. Author manuscript; available in PMC 2016 March 01.

Published in final edited form as:

J Invest Dermatol. 2015 September ; 135(9): 2309–2318. doi:10.1038/jid.2015.94.

Fidgetin-like 2: a microtubule-based regulator of wound healing

Rabab A. Charafeddine[1], **Joy Makdisi**[2], **David Schairer**[2], **Brian P. O'Rourke**[1], **Juan D. Diaz-Valencia**[1], **Jason Chouake**[2], **Allison Kutner**[2], **Aimee Krausz**[2], **Brandon Adler**[2], **Parimala Nacharaju**[1], **Hongying Liang**[1], **Suranjana Mukherjee**[1], **Joel M. Friedman**[1], **Adam Friedman**[2,†], **Joshua D. Nosanchuk**[2,†], and **David J. Sharp**[1,*,†]

[1]Department of Physiology and Biophysics, Albert Einstein College of Medicine, 1300 Morris Park Avenue, Bronx, NY 10461

[2]Department of Medicine, Albert Einstein College of Medicine, 1300 Morris Park Avenue, Bronx, NY 10461

Abstract

Wound healing is a complex process driven largely by the migration of a variety of distinct cell types from the wound margin into the wound zone. In this study, we identify the previously uncharacterized microtubule-severing enzyme, Fidgetin-like 2 (FL2), as a fundamental regulator of cell migration that can be targeted *in vivo* using nanoparticle-encapsulated siRNA to promote wound closure and regeneration. *In vitro,* depletion of FL2 from mammalian tissue culture cells results in a more than two-fold increase in the rate of cell movement, due in part to a significant increase in directional motility. Immunofluorescence analyses indicate that FL2 normally localizes to the cell edge, importantly to the leading edge of polarized cells, where it regulates the organization and dynamics of the microtubule cytoskeleton. To clinically translate these findings, we utilized a nanoparticle-based siRNA delivery platform to locally deplete FL2 in both murine full-thickness excisional and burn wounds. Topical application of FL2 siRNA nanoparticles to either wound type results in a significant enhancement in the rate and quality of wound closure both clinically and histologically relative to controls. Taken together, these results identify FL2 as a promising therapeutic target to promote the regeneration and repair of cutaneous wounds.

Keywords

wound healing; microtubules; severing enzymes; Fidgetin-like 2; siRNA encapsulated nanoparticles

*Correspondence should be addressed to david.sharp@einstein.yu.edu.
†Co-senior author

Introduction

Though wound healing is orchestrated largely by the migration of diverse cell types from the wound edge into the wound zone, the intracellular mechanisms that drive cell migration have not yet been effectively harnessed for therapeutic purposes. A potentially ideal target in this regard is the microtubule (MT) cytoskeleton. MTs are highly dynamic, polar polymers of tubulin with a fast growing plus-end and slower growing minus-end. Within cells, MTs are organized into extremely plastic higher order arrays with their plus-ends generally facing the cell periphery and minus-ends oriented towards the nucleus. While MTs are not required for cell migration *per se*, there is growing evidence that they control and coordinate multiple parameters of cell movement including actin based membrane protrusions (Wehrle-Haller and Imhof 2003; Gardel et al. 2011), the assembly and organization of integrin based focal adhesion complexes (FAs) (Kaverina et al. 1998; Stehbens and Wittmann 2012) and the distribution and delivery of Golgi-derived and endosomal vesicles to the leading edge (Watanabe et al. 2005; Kaverina and Straube 2011).

We recently showed that the migration of *Drosophila melanogaster* cells was strongly enhanced by the RNAi-mediated depletion of the MT regulatory protein Katanin (Zhang et al. 2011). Katanin is a conserved member of the ATPases associated with diverse cellular activities (AAA) protein superfamily (Roll-Mecak and McNally 2010; Sharp and Ross 2012), which displays the capacity to sever and depolymerize MT plus-ends *in vitro* (McNally and Vale 1993). In *Drosophila*, Katanin localizes to the cell cortex and normally suppresses cell movement by locally destroying MTs (Zhang et al. 2011). Though Katanin does not regulate the migration of most mammalian cells, our findings raised the intriguing possibility that a related but as of yet undetermined MT severing enzyme could be similarly targeted to promote cell migration and wound healing in mammals.

We show here that a related but presently uncharacterized protein, Fidgetin-like 2 (FL2), can be targeted to strongly enhance the wound healing behavior of mammalian cells, and in particular skin cells, both *in vitro* and *in vivo*. We previously reported that Fidgetins function as MT severing and depolymerizing enzymes (Zhang et al. 2007; Mukherjee et al. 2012). siRNA-mediated depletion of FL2 induces a more than 2-fold increase in the rates of *in vitro* cell movement and *in vivo* wound closure. When functioning normally, FL2 localizes to regions of the cell cortex, suppresses MT growth, and regulates the size and distribution of FA complexes, likely through its impact on MT dynamics. Finally, we present an innovative nanoparticle-based topical siRNA delivery system that has allowed us to efficiently reduce the expression of FL2 in murine wounds and accelerate wound healing.

Results

FL2 is a regulator of cell migration in vitro

Our interest in FL2 as a potential therapeutic target for wound healing initiated from a siRNA-based screen for MT severing or depolymerizing enzymes that regulate human cell motility. This screen targeted all of the known or putative MT severing or depolymerizing enzymes encoded by the human genome and the effect of siRNA treatment on the migration of cultured U2OS cells (human osteosarcoma cells) was measured using a standard in vitro

scratch assay. Of all targets analyzed in this screen, depletion of the previously uncharacterized protein, FL2, had the most pronounced effect on cellular behavior. A decrease in FL2 mRNA and protein levels following siRNA treatment was confirmed using qPCR and western blotting, respectively. (Supplemental Figure S1a and c). In particular, FL2 siRNA treatment induced a statistically significant, ~2.5-fold increase in the rate of scratch closure (Figure 1a and b; Movie S1) due largely to enhanced cell migration into the cell-free scratch zone. Quantification of the movement trajectories of isolated individual cells indicated Fl2 siRNA-treatment caused cells to move significantly faster and more directionally than controls (Figure 1c and d). The increased rate of cell migration caused by FL2 knockdown was rescued to control levels when FL2 siRNA-treated cells were induced to express an exogenous GFP-FL2 construct (which lacks the 3' UTR sequences targeted by our siRNA), ruling out off-target effects (Supplemental Figure S2a). Finally, a qualitatively similar enhancement of cell migration after FL2 siRNA treatment was observed in a human keratinocyte cell line (HaCaT) and a mouse fibroblast cell line (L929) (Figure 1d; Supplemental Figure S3). Thus, FL2 normally functions to suppress cell motility in a variety of cell types relevant to mammalian cutaneous wound healing.

It should be noted that a small but statistically significant increase in the proliferation rates of FL2-depleted U2OS and L929 cells (but not HaCaTs) was also observed in our studies (Supplemental Figure S4). However, we do not believe that this can account for the enhancements of cell migration described above since migration measurements (Figure 1d; Supplemental Figure S2a and S3a) were performed on isolated cells that did not undergo mitosis during the analysis time-course and were not pushed forward by a proliferating cell mass (e.g. at the scratch edge). The potential mechanisms by which FL2 influences the proliferation of some cell types will be explored in a separate study.

FL2 localizes to and regulates the organization of MTs at the cell cortex

As a first step towards understanding the mechanistic basis of FL2's impact on cell motility, we examined its subcellular distribution using indirect immunofluorescence. Multiple monoclonal antibodies raised against different regions of FL2 showed a strong enrichment at the cortex of U2OS cells with similar staining patterns observed in HaCaTs and L929s. This cortical labeling was generally discontinuous and most pronounced at the leading edge/lamellipodium of polarized cells where it often became particularly concentrated at sites where individual microtubule ends contacted the cortex (Figure 1e). siRNA treatment significantly reduced the intensity of cortical FL2 immunostaining supporting the specificity of this localization pattern (Supplemental Figure S5). Moreover, exogenously expressed GFP-FL2 acquired a similar cortical localization (Supplemental Figure S6). By Western blot, our antibodies primarily labeled a tight doublet running between 65 and 75kD (Supplemental Figure S1b). The predicted molecular mass of FL2 is 66kD. This doublet was substantially reduced after FL2 siRNA treatment strongly supporting the hypothesis it corresponds to native FL2 and that FL2 protein levels are reduced by siRNA treatment (Supplemental Figure S1c).

We next tested the hypothesis that FL2 impacts cell motility via the MT cytoskeleton. Quantitative immunofluorescence performed in U2OS cells, which are particularly suited for

this kind of microscopy, owing to their size and extremely flat morphology, revealed that the depletion of FL2 significantly increased cellular MT polymer levels ~40% relative to controls ($p<0.005$), —an expected outcome if FL2 normally functions by destabilizing MTs. This siRNA phenotype was rescued by exogenously expressed GFP-FL2 (Supplemental Figure S2b). Depletion of FL2 also induced the formation of dense MT bundles just beneath the cell edge consistent with the protein's cortical localization (Figure 2a and b). Additionally, cells with reduced FL2 displayed a decrease in acetylated MTs (Figure 2c and d). Acetylation is a posttranslational modification that usually marks a slow-growing stable MT subpopulation (Hammond et al. 2008), thus suggesting that FL2 normally acts on dynamic, non-acetylated MTs. This is in contrast to Katanin which preferentially severs acetylated MTs (Sudo and Baas 2010).

In a parallel line of study, we examined how the loss of FL2 affects MT dynamics and organization by immunostaining for EB1, a protein that specifically labels growing MT plus-ends. MT-associated EB1 staining normally acquires a comet-like appearance because the protein associates with tubulin subunits as they are incorporated into the MT end and then dissociates shortly thereafter (Vaughan 2005). Immunofluorescence analysis showed a significant increase in the average number of EB1 comets at the cell edge following FL2 knockdown, further supporting the hypothesis that FL2 locally targets dynamic MTs (Figure 3 a and b). Moreover, the mean length of EB1 comets was significantly increased after FL2 knockdown, suggesting an increase in MT growth rate (Figure 3b). Tracking of GFP-EB1 comet movement in living cells is standardly used to directly assess alterations in MT dynamics. Unfortunately, this approach was insufficient to track the elongated GFP-EB1 comets induced by FL2 siRNA. Regardless, our data clearly demonstrate that FL2 is an important regulator of the MT cytoskeleton in migratory cells. A similar increase in EB1 comet number and length as well as a decrease in the density of acetylated MTs was also observed in HaCaTs (Figure 3b; Supplemental Figure S7a).

FL2 impacts FA size and maturity

Integrin-based FAs are integral factors in the migration of large cells such as fibroblasts and keratinocytes (Wehrle-Haller and Imhof 2003). In view of the fact that growing MTs at the leading edge target and regulate the assembly/disassembly of FAs (Kaverina et al. 1998; Ezratty et al. 2005; Efimov et al. 2008), we examined how the depletion of FL2 impacted the distribution and morphology of FAs at the cell edge. Immunofluorescence measurements of vinculin, a component of the FA complex, revealed a significant increase in the average area of FAs in FL2-depleted U2OS cells compared to controls (0.87 ± 0.07 m^2 in controls vs. 2.54 ± 0.18 m^2 in FL2 siRNA-treated cells; Figure 3 c and d). Though FA area has long been thought to negatively correlate with migration speed (Gardel et al. 2011), recent reports have identified a biphasic relationship in which cells move faster with increased FA area up to a threshold point, beyond which cell migration slows down (Kim and Wirtz 2013a, 2013b). Strikingly, the average area of FAs in FL2 depleted cells, $2.54\mu m^2$, is almost identical to the FA area shown by Kim and Wirtz to correlate with the fastest migration speed in fibroblasts (Kim and Wirtz 2013a). FA area was restored to control levels in FL2 siRNA-treated U2OS cells expressing GFP-FL2 (Supplemental Figure S2b and c). HaCaTs showed a similar increase in FA area following FL2 knockdown (Supplemental Figure S7b).

FL2 can be targeted to promote wound closure and regeneration in vivo

To translate the effects of modulating FL2 expression to a more physiologically and medically significant model, we investigated whether FL2 depletion can affect cell migration during cutaneous wound healing in excisional murine wounds (Martinez et al. 2009). Using a previously described nanoparticle platform (Friedman et al. 2008; Cabrales et al. 2010), we successfully encapsulated FL2 siRNA (NPsi) to locally and effectively deliver intact siRNA to the wound site. After subjecting the dorsa of BALB/c mice to 4 mm full-thickness excisional wounds, suspensions of FL2 NPsi were topically applied directly to the wounds at either day 0 or days 0 and 2, and the rates of wound closure were assessed relative to controls (non-targeting control NPsi or untreated wounds). Wounds were splinted with Tegaderm™ to minimize closure by contraction (common in rodent wound models), an approach that in our hands is comparable to glued or sutured rigid supports but produces fewer adjacent tissue alterations. The data plotted in Figure 4 represents wound area relative to the initial wound area on day zero. Measurements of wounds throughout the wound healing process demonstrated that FL2 NPsi significantly accelerated wound closure *in vivo* with either a single application after wounding (Figure 4a) or treatment on day 0 and 2 (Figure 4b). The addition of a second treatment at day 2 after wounding further accelerated the resolution of the excisional injury, demonstrating that the cells were not refractory to RNAi and that the process of healing could be further beneficially manipulated. FL2 NPsi-treated excisional wounds healed faster and remained smaller than control wounds throughout the experiment. In addition, to confirm *in vivo* FL2 knock down, RNA was extracted from treated wounds and measured by quantitative PCR, which showed a significant decrease in FL2 expression at both 2 and 8 days after FL2 NPsi treatment compared to controls (Figure 4c).

We further evaluated the effects of FL2 NPsi on wound healing in a murine thermal burn wound model (Macherla et al. 2012; Sanchez et al. 2014). In contrast to excision wounds, full thickness thermal burn wounds are more traumatic secondary to heat-induced tissue coagulation, and healing is slower due to the edema, extensive necrosis, and hypoxia (Benson et al. 2006). Nevertheless, as with excision wounds, burns treated topically with FL2 NPsi closed significantly faster than untreated controls (Supplemental Figure S8a and b). Control NPsi did not enhance and even slightly attenuate burn closure relative to controls (Supplemental Figure S9) and thus were not used in this study. Quantitative PCR from wound sections also confirmed a decrease in FL2 mRNA levels after FL2 NPsi treatment (Supplemental Figure S8c).

FL2 knockdown enhances the quality of wound healing

To further examine wound morphology, histopathologic analyses were performed on formalin-fixed sections of NPsi-treated and control wounds. On day 7, hematoxylin and eosin staining of control excisional wounds (Figure 5a) demonstrated a thin layer of re-epithelialized epidermis with overlying mounds of serum crust. The dermis was composed of inflammatory, disorganized granulation tissue without evidence of subcutis. This histopathology was indicative of a disorganized wound, early in the proliferative phase of wound healing. The residual wound areas at both time intervals were readily distinguishable from the adjacent intact tissues. In marked contrast, FL2 NPsi-treated excisional wounds

(Figure 5a) had completely re-epithelialized the epidermis by day 7 with overlying, organized basket weaving stratum corneum. The dermis was devoid of intense inflammation, and was infiltrated with parallel fibroblasts. A healthy appearing subcutis was also present. The histopathology seen in FL2 NPsi-treated wounds was indicative of a well-healed, organized scar. By day 10, further restoration of normal tissue architecture, including higher order structures such as hair follicles, is clearly visible in the FL2 NPsi treated wound but remain absent in controls (Figure 5a).

In the control excisional day 7 wounds (Figure 5b), Masson's trichrome staining for collagen revealed necrotic, degenerated collagen with minimal pale, newly deposited collagen in the wound bed. In contrast, analysis of the NPsi-treated wounds revealed homogenous, well-organized, newly formed collagen that stains light blue, and there was minimal cell death as indicated by the lack of red staining (Figure 5b). At day 10, collagen deposition in the control wounds remained disorganized and rudimentary, while the FL2 NPsi-treated wounds demonstrated ordered, mature collagen deposition (Figure 5b). Similar results were identified in burn wounds at day 10 and 13 after injury (Supplemental Figure S10). The assessments at the later time intervals were performed as re-epithelialization and organization of the tissue at a histopathologic level takes longer in a burn wound as compared to an excisional injury.

Discussion

The results described herein indicate that regulation of MT function via FL2 NPsi is an innovative approach to the treatment of various cutaneous wounds including cuts and burns. Our complementary in vitro and in vivo studies strongly support the hypothesis that localized depletion of Fidgetin-like 2 induced by the topical application of FL2 NPsi enhances wound closure and re-epithelialization by stimulating the migration of keratinocytes and fibroblasts into the wound from the surrounding skin. The normal regulation of FL2 during wound regeneration and repair is an area ripe for future study as is its potential dysregulation in chronic wounds.

FL2: an important regulator of the MTs cytoskeleton and cell motility

A major strength of this study is the utilization of basic cell biology to identify a clear and specific intracellular mechanism of action for this potential therapeutic target. In particular, FL2's cortical localization, along with the increases in MT polymer mass and bundling at the cell edge that follow its depletion by siRNA, strongly support the hypothesis that FL2 normally suppresses cell migration by selectively shearing MTs that contact specific sites at the cell cortex, most notably at the leading edge. We assume that FL2 functions as a MT severing enzyme because of its close relationship to Fidgetin, a known MT severing enzyme and depolymerase (Mukherjee et al. 2012), though this will require further experimental validation. We recently showed that *Drosophila melanogaster* cells utilize another MT severing enzyme, Katanin, in much the same way, indicating this to be an evolutionarily conserved pathway (Zhang et al. 2011).

How do the alterations in MT growth and organization at the cell edge caused by the depletion of FL2 translate into increased cellular motility? There is now a good deal of

evidence to indicate that localized shifts in MT assembly/disassembly at the leading edge modulate larger regulatory pathways that control actin organization/dynamics and FA assembly/maturation (Wehrle-Haller and Imhof 2003; Kaverina and Straube 2011). Though our data are inconclusive with regard to FL2's impacts on actin (not shown), we have found that FL2 strongly and significantly influences FAs. Indeed, depletion of FL2 appears to activate a shift in FA size that is optimal for cell migration. Further work will be required to determine precisely how FL2 and MTs are linked to this shift. However, reasonable, non-exclusive possibilities include 1) localized changes in the balance of activities of members of the Rho family of small GTPases, which have been found to be both sensitive to altered MT dynamics (Krendel et al. 2002; Wittmann et al. 2003; Wen et al. 2004) and to control FA assembly (Rooney et al. 2010; Stehbens and Wittmann 2012), or 2) modulation of the motor-driven transport of FA components and regulators along MT tracks (Miller et al. 2009; Falnikar et al. 2011).

It is notable that FL2's localization at the cell front is shared by several MT stabilizers involved in actin polymerization and FA turnover (Watanabe et al. 2005). These include APC, ACF7, and CLASPs. Depletion of these stabilizers inhibits cell migration in various cell types (Wen et al. 2004; Wittmann and Waterman-Storer 2005; Barth et al. 2008; Wu et al. 2008, 2011; Stramer et al. 2010), implying a functional antagonism with FL2. Research in this area may lead to novel approaches for precisely controlling cell motility in a number of different therapeutic contexts.

An innovative RNAi-based nanotherapeutic approach to promote wound healing

Nanoscale drug delivery vehicles operate exceptionally well as topical therapeutics due to their distinctive physical characteristics such as high surface-to-volume ratio as a result of their small size (Nasir 2010). These properties confer the ability to traverse the biological barrier of the skin and allow for rapid delivery of key biomolecules (Blecher et al. 2012). Of particular interest within our study, nanoparticle drug platforms are also promising for the topical delivery of siRNA, which cannot be delivered as a therapeutic modality in its naked form because it is susceptible to degradation by endogenous enzymes, and because its large size and negative charge hamper its ability to cross lipophilic cellular membrane (Castanotto and Rossi 2009). Moreover, we found no evidence of toxicity of the nanoparticles (Friedman et al. 2008; Han et al. 2009) and encapsulation of the siRNA likely minimizes interaction with innate immune receptors (Robbins et al. 2009). Capitalizing on the attributes of nanomaterials, our findings reveal that FL2 NPsi has the potential to serve as a topical modality for wound healing by accelerating wound closure as well as enhancing the maturation rate of the wound structure.

Materials and Methods

Antibody production

Monoclonal antibodies against human FIGNL2 (NM_001013690) were generated in mice (Abmart) using the following peptides: antiFL2-1 (SSTTPSPAHK) antiFL2-2 (TPEHAQPLNQ) antiFL2-3 (SGETPKGVDP).

Commercial antibodies

We used the following antibodies for immunofluorescence: mouse anti-tubulin (Fisher Scientific, MS581P1), rabbit anti-tubulin (Abcam, Ab18251), mouse anti-acetylated tubulin (Sigma, T6793), mouse anti-EB1 (BD Transduction Laboratories, 610534), mouse anti-vinculin (Abcam, ab18058), Cy2-conjugated Anti-mouse IgG, Cy2-conjugated Anti-Rabbit IgG, Rhodamine Anti-mouse IgG, and Rhodamine Anti-Rabbit IgG (Jackson Laboratories).

Plasmid construction and expression

The N-terminal GFP-tagged construct of FL2 was constructed from pANT7_cGST (DNASU clone: HsCD00403041) and subcloned into pEGFP-C1. The construct was expressed in U2OS using Lipofectamine 2000 (Invitrogen, 11668027). 24 h after plasmid transfection, U2OS cells were fixed and labelled with anti-GFP antibody (Abcam, ab290).

Cell culture and siRNA treatment

U2OS, U2OS-EB1 (a gift from Dr. Pavel Draber (Vinopal et al. 2012)), and HaCaT (a gift from Dr. Paul Higgins) cells were cultured in DMEM (Invitrogen, 11965092) supplemented with 10% fetal bovine serum and 1% Glutamax at 37°C in the presence 5% CO2. L929s (a gift from Dr. Bin Zhou) were cultured in EMEM (ATCC, 30–3000) and 10% FBS, under the same conditions.

For *in vitro* FL2 knock down studies, cells were transfected using 2.5 μl Lipofectamine RNAiMAX (Invitrogen, 13778075) or 7.5 Lipofectamine 3000 with 40 or 75 pmol, respectively, of either FL2 siRNA (Dharmacon, ON-TARGETplus set of four), mouse FL2 (Sigma-Aldrich, SASI_Mm02_00354635), or a negative control siRNA (Sigma-Aldrich, SIC001).

For FL2 rescue experiments, 24 h after siRNA treatment, U2OS cells were transfected with 1.5 μg of either pEGFP-C1 or pEGFP-FL2 using 4 μl of Lipofectamine 2000. Media was replaced 5 h later and cells were processed the next day depending on the experiments (see below).

Unless otherwise noted, experiments in U2OS cells were repeated 3 times and experiments in HaCaT and L929 cells were repeated twice, independently.

In vitro scratch and single cell migration assays

For scratch assays, cell monolayers were scratched 48 h after siRNA treatment (24 h after plasmid expression for FL2 rescue experiments) with a 200μl pipette tip. For single cell migration assays, HaCaTs were plated at low cell density to allow for single cell movement. Cell migration was imaged by time-lapse microscopy at 20–30 min intervals overnight in an environmental chamber using an Inverted Olympus IX71 microscope with a 10× (0.3 NA) objective and a Photometrics CoolSnap HQ CCD camera. Movies were analyzed using ImageJ and individual cells were tracked with its Manual Tracking plugin. The migration rate was calculated by either dividing the change in the area by length of the fixed image edge and finally by the number of hours or by tracking individual cells. Analysis of the cell tracks was done using DiPer (Gorelik and Gautreau 2014).

Proliferation Assay

24h before siRNA treatment, equal amounts of cells were plated in triplicates in either 6 or 24-well plates. Cells were detached and counted 24, 48, and 72 h after siRNA treatment using a hemocytometer.

Quantitative PCR

Unless otherwise noted, supplies for RNA quantification were purchased from Life Technologies. For tissue culture samples, mRNA was extracted using the Purelink RNA mini kit (12183018A). cDNA was synthesized the same day using the SuperScript III First-strand synthesis system (18080051). qPCR was done using TaqMan Universal Master Mix II (4440040) with TaqMan hFIGNL2 primers (4448892). hGAPDH was used as a control (4331182).

Alternatively, for mouse skin wound samples, the skin of control and FL2NPsi-treated wounds was excised at day 2 and 8 after wounding. Trizol (15596-026) was used to pulverize the tissue and a standard RNA extraction protocol was followed. cDNA synthesis was performed as described above. qPCR was done using PowerSybr green Master Mix with mFIGNL2 primers and mGAPDH (IDT) or mActin (IDT) were used as loading controls. The cDNA was amplified using the 7300 Real-Time PCR system (Applied Biosystems). Resulting data were quantified using the comparative $2^{-\Delta\Delta Ct}$ method. The average of control skin wounds was normalized to 1 and used for relative quantification.

Western Blotting

Western blot analysis was done using cells frozen 72 h after siRNA treatment as described in (O'Rourke et al. 2014).

Immunofluorescence microscopy

Cells were grown on coverslips for 48 h after siRNA treatment (18 h after plasmid expression for FL2 rescue experiments) and then fixed for 10 minutes with a fixative solution (4% paraformaldehyde, 0.1% Triton X, and 0.15% glutaraldehyde in BRB80) and a standard immunolabeling protocol was followed.

Cells were imaged using a 4D spinning-disk confocal microscope (PerkinElmer) with either a 40× (1.3 NA), a 60× (1.4 NA), or a 100× (1.4 NA) objective and a digital camera (Orca ER; Hamamatsu). Z planes= 0.5 μm.

Nanoparticle encapsulated siRNA preparation

Five hundred μl of Tetramethyl orthosilicate (TMOS) was hydrolyzed in the presence of 100 μl of 1 mM HCl by sonication on ice for about 15 min, until a single phase formed. The hydrolyzed TMOS (100 μl) was added to 900 μl of 20 μM of siRNA (mouse FL2 (Sigma-Aldrich, SASI_Mm02_00354635) or the negative control) solution containing 10 mM phosphate, pH 7.4. A gel was formed within 10 minutes. The gel was frozen at −80°C for 15 minutes and lyophilized.

In vivo experiments

Animal experiments were performed according to the guidelines published by the Institute of Laboratory Animal Resources of National Research Council and animal care for this study was approved by the Institutional Animal Care and Use Committee of the Albert Einstein College of Medicine. Two murine wound models were utilized: a full thickness wound model and a thermal burn wound model. Prior to procedures, mice were anesthetized with a ketamine-xylazine cocktail. The dorsa of Balb/c mice (6–8 weeks; National Cancer Institute, Frederick, MD) were depilated and wounded with either a 4mm punch biopsy (Integra Miltex, York, PA) or a thermal burn. Uniform, reproducible burn wounds were produced with a heated brass knob (1.27 cm diameter; 45 seconds until reaching 180°–200°C measured by calorimeter). Wounds were splinted with Tegaderm™ in which circular openings were created to enable the dressings to be seated immediately adjacent to the wounds. Nuclease-free water was used to suspend the NPsi. Using a micropipette, nuclease-free water alone, non-targeting NPsi or FL2 NPsi was topically applied to the wound beds in single doses (100 pmol of siRNA) immediately after wounding on day 0 or at both day 0 and 2. Control groups were either treated with non-targeting NPsi on a schedule correlating with the FL2 NPsi or were not treated. Wounds were serially photographed and measured independently by two readers using calipers to track the progression of wound closure. Mice were randomly selected for sacrifice on designated days and tissue from the wounds was excised for both PCR and histopathologic analysis. For histopathology, tissue was embedded in paraffin, sectioned in 10 μm sections, and stained with hematoxylin and eosin or Masson's trichrome.

Supplementary Material

Refer to Web version on PubMed Central for supplementary material.

Acknowledgements

The authors would like to thank Lisa Baker for production and purification of the FL2 antibodies and Drs. Bin Zhou and Peter Baas for helpful discussions.

Conflict of Interest:

David J. Sharp and Rabab A. Charafeddine are co-inventors on US Patent #20130022667 entitled "Fidgetin-like 2 as a target to enhance wound healing" which has been licensed by MicroCures Inc. Dr. Sharp is currently CSO of MicroCures. The research presented in this manuscript was funded by grants from the DoD and NIH—no research funding was provided by MicroCures.

References

Barth AIM, Caro-Gonzalez HY, Nelson WJ. Role of adenomatous polyposis coli (APC) and microtubules in directional cell migration and neuronal polarization. Cell Shape Tissue Morphog. 2008; 19:245–251.

Benson A, Dickson WA, Boyce DE. Burns. BMJ. 2006; 332:649–652. [PubMed: 16543335]

Blecher K, Martinez LR, Tuckman-Vernon C, et al. Nitric oxide-releasing nanoparticles accelerate wound healing in NOD-SCID mice. Nanomedicine Nanotechnol Biol Med. 2012; 8:1364–1371.

Cabrales P, Han G, Roche C, et al. Sustained release nitric oxide from long-lived circulating nanoparticles. Free Radic Biol Med. 2010; 49:530–538. [PubMed: 20460149]

Castanotto D, Rossi JJ. The promises and pitfalls of RNA-interference-based therapeutics. Nature. 2009; 457:426–433. [PubMed: 19158789]

Efimov A, Schiefermeier N, Grigoriev I, et al. Paxillin-dependent stimulation of microtubule catastrophes at focal adhesion sites. J Cell Sci. 2008; 121:196–204. [PubMed: 18187451]

Ezratty EJ, Partridge MA, Gundersen GG. Microtubule-induced focal adhesion disassembly is mediated by dynamin and focal adhesion kinase. Nat Cell Biol. 2005; 7:581–590. [PubMed: 15895076]

Falnikar A, Tole S, Baas PW. Kinesin-5, a mitotic microtubule-associated motor protein, modulates neuronal migration. Mol Biol Cell. 2011 mbc.E10–1 – 0905.

Friedman AJ, Han G, Navati MS, et al. Sustained release nitric oxide releasing nanoparticles: Characterization of a novel delivery platform based on nitrite containing hydrogel/glass composites. Nitric Oxide. 2008; 19:12–20. [PubMed: 18457680]

Gardel ML, Schneider IC, Aratyn-Schaus, et al. Mechanical Integration of Actin and Adhesion Dynamics in Cell Migration. Annu Rev Cell Dev Biol. 2011; 26:315–333. [PubMed: 19575647]

Gorelik R, Gautreau A. Quantitative and unbiased analysis of directional persistence in cell migration. Nat Protoc. 2014; 9:1931–1943. [PubMed: 25033209]

Hammond JW, Cai D, Verhey KJ. Tubulin modifications and their cellular functions. Cell Struct Dyn. 2008; 20:71–76.

Han G, Martinez LR, Mihu MR, et al. Nitric Oxide Releasing Nanoparticles Are Therapeutic for Staphylococcus aureus Abscesses in a Murine Model of Infection. PLoS ONE. 2009; 4:e7804. [PubMed: 19915659]

Kaverina I, Rottner K, Small JV. Targeting, Capture, and Stabilization of Microtubules at Early Focal Adhesions. J Cell Biol. 1998; 142:181–190. [PubMed: 9660872]

Kaverina I, Straube A. Regulation of cell migration by dynamic microtubules. Mechanochemical Cell Biol Dev Endothel Action. 2011; 22:968–974.

Kim D-H, Wirtz D. Focal adhesion size uniquely predicts cell migration. FASEB J. 2013a; 27:1351–1361. [PubMed: 23254340]

Kim D-H, Wirtz D. Predicting how cells spread and migrate: Focal adhesion size does matter. Cell Adhes Migr. 2013b; 7:293–296.

Krendel M, Zenke FT, Bokoch GM. Nucleotide exchange factor GEF-H1 mediates cross-talk between microtubules and the actin cytoskeleton. Nat Cell Biol. 2002; 4:294–301. [PubMed: 11912491]

Macherla C, Vellozzi EM, Friedman AJ, et al. Nitric oxide releasing nanoparticles for treatment of Candida albicans burn infections. Front Fungi Their Interact. 2012; 3:193.

Martinez LR, Han G, Chacko M, et al. Antimicrobial and Healing Efficacy of Sustained Release Nitric Oxide Nanoparticles Against Staphylococcus Aureus Skin Infection. J Invest Dermatol. 2009; 129:2463–2469. [PubMed: 19387479]

McNally FJ, Vale RD. Identification of katanin, an ATPase that severs and disassembles stable microtubules. Cell. 1993; 75:419–429. [PubMed: 8221885]

Miller PM, Folkmann AW, Maia ARR, et al. Golgi-derived CLASP-dependent microtubules control Golgi organization and polarized trafficking in motile cells. Nat Cell Biol. 2009; 11:1069–1080. [PubMed: 19701196]

Mukherjee S, Valencia JDD, Stewman S, et al. Human Fidgetin is a microtubule severing the enzyme and minus-end depolymerase that regulates mitosis. Cell Cycle. 2012; 11:2359–2366. [PubMed: 22672901]

Nasir A. Nanodermatology: a bright glimpse just beyond the horizon - part I. Skin Ther Lett. 2010; 15:1–4.

O'Rourke BP, Gomez-Ferreria MA, Berk RH, et al. Cep192 Controls the Balance of Centrosome and Non-Centrosomal Microtubules during Interphase. PLoS ONE. 2014; 9:e101001. [PubMed: 24971877]

Robbins M, Judge A, MacLachlan I. siRNA and innate immunity. Oligonucleotides. 2009; 19:89–102. [PubMed: 19441890]

Roll-Mecak A, McNally FJ. Microtubule-severing enzymes. Curr Opin Cell Biol. 2010; 22:96–103. [PubMed: 19963362]

Rooney C, White G, Nazgiewicz A, et al. The Rac activator STEF (Tiam2) regulates cell migration by microtubule-mediated focal adhesion disassembly. EMBO Rep. 2010; 11:292–298. [PubMed: 20224579]

Sanchez DA, Schairer D, Tuckman-Vernon C, et al. Amphotericin B releasing nanoparticle topical treatment of Candida spp. in the setting of a burn wound. Nanomedicine Nanotechnol Biol Med. 2014; 10:269–277.

Sharp DJ, Ross JL. Microtubule-severing enzymes at the cutting edge. J Cell Sci. 2012; 125:2561–2569. [PubMed: 22595526]

Stehbens S, Wittmann T. Targeting and transport: How microtubules control focal adhesion dynamics. J Cell Biol. 2012; 198:481–489. [PubMed: 22908306]

Stramer B, Moreira S, Millard T, et al. Clasp-mediated microtubule bundling regulates persistent motility and contact repulsion in Drosophila macrophages in vivo. J Cell Biol. 2010; 189:681–689. [PubMed: 20457764]

Sudo H, Baas PW. Acetylation of Microtubules Influences Their Sensitivity to Severing by Katanin in Neurons and Fibroblasts. J Neurosci. 2010; 30:7215–7226. [PubMed: 20505088]

Vaughan KT. TIP maker and TIP marker; EB1 as a master controller of microtubule plus ends. J Cell Biol. 2005; 171:197–200. [PubMed: 16247021]

Vinopal S, Černohorská M, Sulimenko V, et al. γ-Tubulin 2 Nucleates Microtubules and Is Downregulated in Mouse Early Embryogenesis. PLoS ONE. 2012; 7:e29919. [PubMed: 22235350]

Watanabe T, Noritake J, Kaibuchi K. Regulation of microtubules in cell migration. Trends Cell Biol. 2005; 15:76–83. [PubMed: 15695094]

Wehrle-Haller B, Imhof BA. Actin, microtubules and focal adhesion dynamics during cell migration. Int J Biochem Cell Biol. 2003; 35:39–50. [PubMed: 12467646]

Wen Y, Eng CH, Schmoranzer J, et al. EB1 and APC bind to mDia to stabilize microtubules downstream of Rho and promote cell migration. Nat Cell Biol. 2004; 6:820–830. [PubMed: 15311282]

Wittmann T, Bokoch GM, Waterman-Storer CM. Regulation of leading edge microtubule and actin dynamics downstream of Rac1. J Cell Biol. 2003; 161:845–851. [PubMed: 12796474]

Wittmann T, Waterman-Storer CM. Spatial regulation of CLASP affinity for microtubules by Rac1 and GSK3β in migrating epithelial cells. J Cell Biol. 2005; 169:929–939. [PubMed: 15955847]

Wu X, Kodama A, Fuchs E. ACF7 Regulates Cytoskeletal-Focal Adhesion Dynamics and Migration and Has ATPase Activity. Cell. 2008; 135:137–148. [PubMed: 18854161]

Wu X, Shen Q-T, Oristian DS, et al. Skin Stem Cells Orchestrate Directional Migration by Regulating Microtubule-ACF7 Connections through GSK3β. Cell. 2011; 144:341–352. [PubMed: 21295697]

Zhang D, Grode KD, Stewman SF, et al. Drosophila katanin is a microtubule depolymerase that regulates cortical-microtubule plus-end interactions and cell migration. Nat Cell Biol. 2011; 13:361–369. [PubMed: 21378981]

Zhang D, Rogers GC, Buster DW, et al. Three microtubule severing enzymes contribute to the "Pacman-flux" machinery that moves chromosomes. J Cell Biol. 2007; 177:231–242. [PubMed: 17452528]

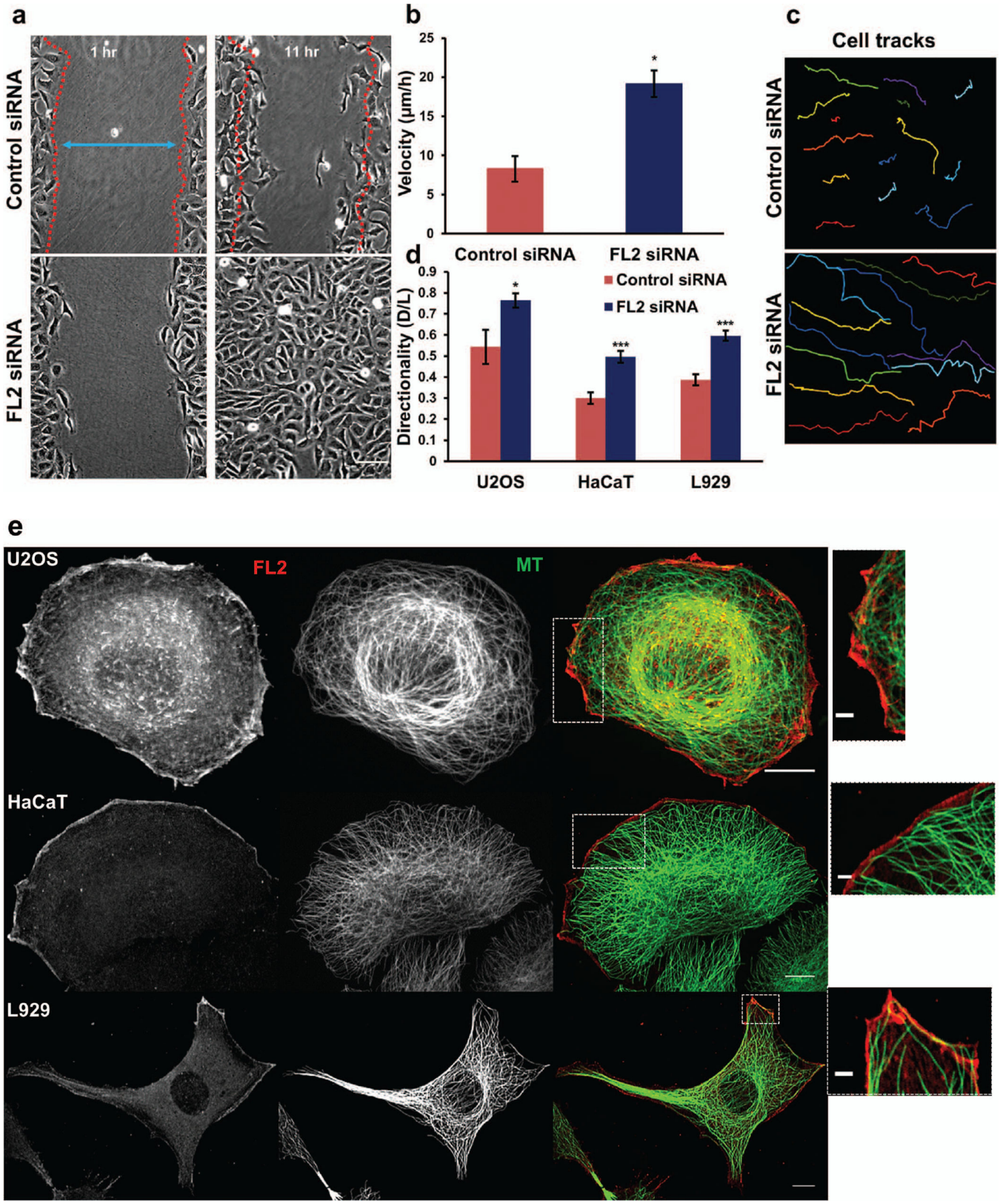

Figure 1. siRNA-mediated depletion of FL2 enhances cell migration

(**a**) Time-lapse images of scratch assays performed with control or FL2 siRNA-treated U2OS cells. Scale bar= 100μm. (**b**) Graphs comparing the average migration rate in control and FL2-depleted cells (n=16 monolayers). (**c**) Trajectories of individual control and FL2-depleted U2OS cells moving from the wound edge into the wound zone. (**d**) Graphs comparing the directionality of migrating control vs. FL2-depleted U2OS (n=34 cells), HaCaT, and L929 (n= 57/83 cells, respectively) cells. D: distance between the start and endpoints. L: total path length. (**e**) Immunofluorescence micrographs of U2OS, HaCaT, and L929 cells double-labeled for FL2 (red) and MTs (green). Scale bar= 10μm. Inset shows a higher magnification of FL2's co-localization with MTs at the cortex. Scale bar= 2μm *, $P<0.05$; ***, $P<0.0005$. mean+/− SEM.

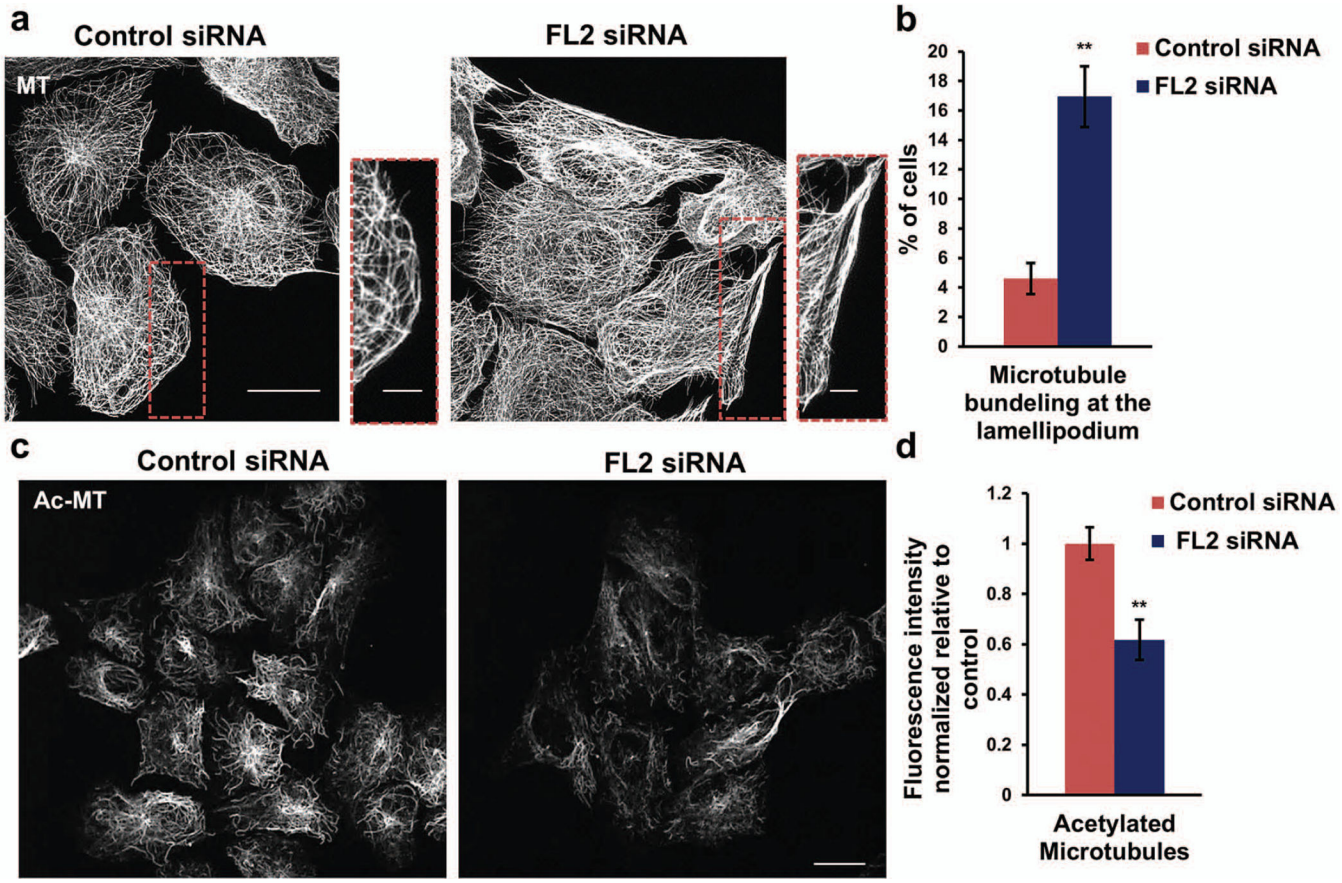

Figure 2. FL2 depletion bundles MTs at the cell edge but reduces their overall stability

(**a**) Immunofluorescence micrographs of control and FL2 siRNA-treated U2OS cells labeled for MTs. Scale bar= 20μm. Insets show higher magnifications of the regions denoted by red boxes. Scale bar= 5μm. (**b**) A graph comparing the percentage of control and FL2 siRNA-treated cells containing dense MT bundles at the cell edge. Data were accumulated from 8 experiments (n=25 cells). (**c**) Immunofluorescence micrographs of control and FL2 siRNA-treated U2OS cells labeled for acetylated MTs (Ac-MT). Scale bar= 20μm. (**d**) Quantitative image analysis of individual cells revealed a significant reduction in Ac-MT levels after FL2 siRNA treatment. Data were accumulated from 7 experiments (n=25 cells each). **, $P<0.005$. mean+/−SEM.

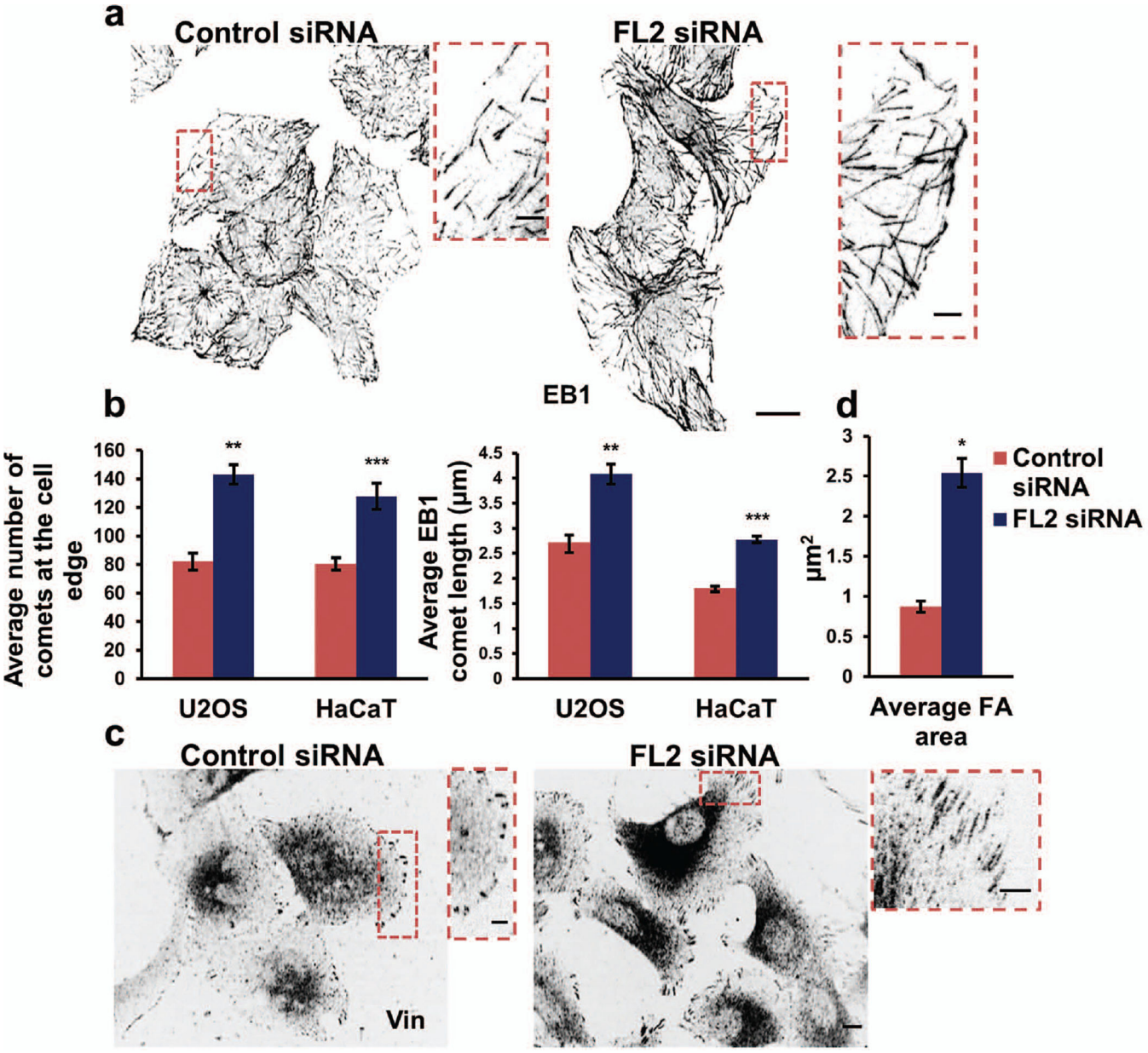

Figure 3. FL2 depletion augments EB1 comet number and length and adhesion size

(**a**) Immunofluorescence micrographs of control and FL2 siRNA-treated U2OS cells labeled for EB1. Scale bar= 20μm. Insets show higher magnifications of the regions denoted by red boxes. Scale bar= 5μm. (**b**) Image analysis of the number (n=10 cells each) and length of EB1 comets (100 comets each) after FL2 depletion in U2OS and HaCaT cells. (**c**) Immunofluorescence micrographs of control and FL2-depleted U2OS cells labeled for the FA marker, vinculin (Vin). Scale bar= 10μm. Insets represent magnified regions of FAs at the cortex. Scale bar=5μm. (**d**) Fluorescence image analysis of control and FL2-depleted U2OS cells measuring average FA area (n=100 FAs each). Images were color inverted. *, P<0.05; **, P<0.005; ***, P<0.0005. mean+/− SEM.

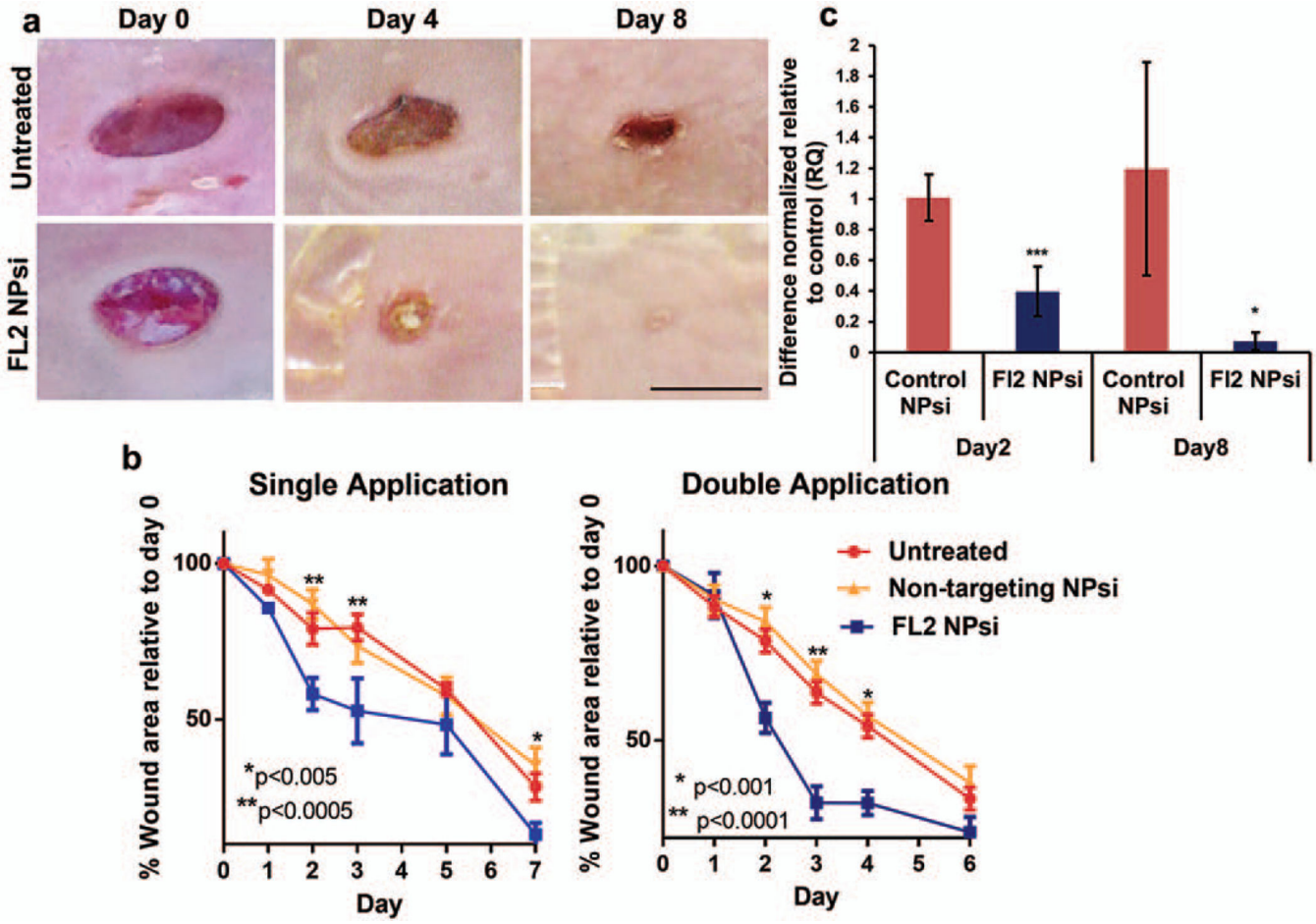

Figure 4. Topical application of FL2 NPsi increases the rate of excision wound closure *in vivo*

(**a**) Representative images showing the closure of untreated and FL2 NPsi-treated murine full thickness biopsy wounds. Scale bar= 4mm. FL2 NPsi was added at days 0 and 2 after wounding. (**b**) Plots comparing the closure of untreated and non-targeting and FL2 NPsi treated wounds. Left: wound closure after a single application of the NPsi at day 0 (n=6). Right: wound closure after a double application of NPsi at days 0 and 2 after wounding (n=20 for each condition on days 0–3; n=16 on days 4–6). (**c**) Quantitative PCR of FL2 mRNA 2 and 8 days after wounding (n=8 wounds). RQ: Relative Quantification.*, P<0.05; **, P<0.005; ***, P<0.0005. mean+/− SEM.

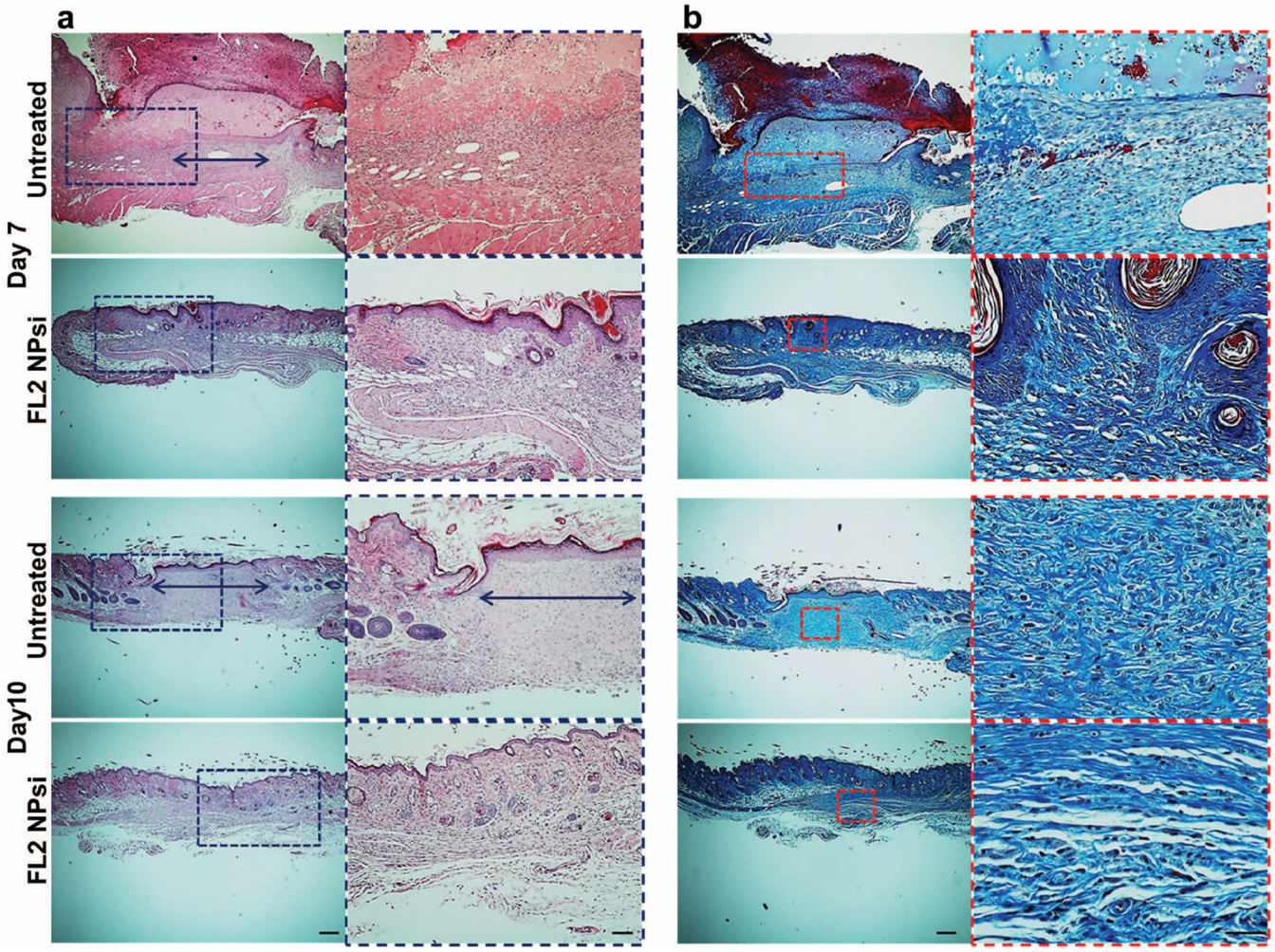

Figure 5. Histopathology sections of excision wounds show an enhancement in wound healing

(**a**) Hematoxylin and eosin staining of skin sections taken 7 and 10 days after wounding. Scale bar= 100μm. Insets show higher magnifications of the regions denoted by blue boxes. Scale bar= 50μm. Double-headed arrows designate observable wound areas. (**b**) Trichrome staining of skin sections taken 7 and 10 days after wounding. Scale bar= 100μm. Insets show higher magnifications of the regions denoted by red boxes. Scale bar= 20μm.